Microstructures and mechanical properties of compositionally complex CO-free $FeNiMnCr_{18}$ FCC solid solution alloy

Z. Wu, H. Bei

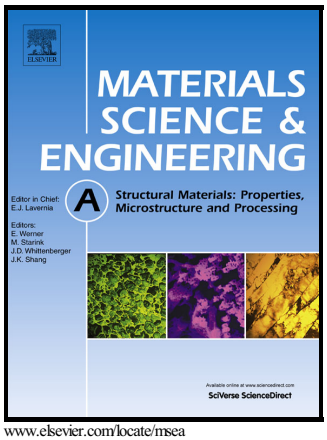

www.elsevier.com/locate/msea

PII: S0921-5093(15)30043-5
DOI: http://dx.doi.org/10.1016/j.msea.2015.05.097
Reference: MSA32425

To appear in: *Materials Science & Engineering A*

Received date: 23 April 2015
Revised date: 26 May 2015
Accepted date: 28 May 2015

Cite this article as: Z. Wu and H. Bei, Microstructures and mechanical properties of compositionally complex CO-free $FeNiMnCr_{18}$ FCC solid solution alloy, *Materials Science & Engineering A*, http://dx.doi.org/10.1016/j.msea.2015.05.097

Microstructures and Mechanical Properties of Compositionally Complex Co-free $FeNiMnCr_{18}$ FCC Solid Solution Alloy

Z. Wu[a, b] and H. Bei[a *]

[a] Materials Science and Technology Division, Oak Ridge National Laboratory, Oak Ridge, TN 37831 USA

[b] Materials Science and Engineering Department, University of Tennessee, Knoxville, TN 37996 USA

Abstract:

Recently, a *structurally-simple but compositionally-complex* FeNiCoMnCr high entropy alloy was found to have excellent mechanical properties (e.g., high strength and ductility). To understand the potential of using high entropy alloys as structural materials for advanced nuclear reactor and power plants, it is necessary to have a thorough understanding of their structural stability and mechanical properties degradation under neutron irradiation. This requires us to develop a similar model alloy without Co because material with Co will make post-neutron-irradiation testing difficult due to the production of high levels of the ^{60}Co radioisotope. To achieve this goal, a FCC-structured single-phase alloy with a composition of $FeNiMnCr_{18}$ was successfully developed and compared with the FeNiCoMnCr high entropy alloy. This near-equiatomic $FeNiMnCr_{18}$ alloy has good malleability and its microstructure can be controlled by thermomechanical processing. By rolling and annealing, the as-cast elongated-grained-microstructure is replaced by homogeneous equiaxed grains. The mechanical properties (e.g., strength and ductility) of the $FeNiMnCr_{18}$ alloy are comparable to those of the equiatomic FeNiCoMnCr high entropy alloy. Both strength and ductility increase with decreasing deformation temperature, with the largest difference occurring between 293 and 77 K. Extensive twin-bands which are bundles of numerous individual twins are observed when it is tensile-fractured at 77 K. No twin bands are detected by EBSD for materials deformed at 293 K and higher. The unusual temperature-dependencies of UTS and uniform elongation could be caused by the development of the dense twin substructure,

twin-dislocation interactions and the interactions between primary and secondary twinning systems which will result in a microstructure refinement and hence cause enhanced strain hardening and postponed necking.

Keywords: Solid solution alloys; Mechanical properties; Hardening; Microstructure; EBSD; High entropy alloy

* Corresponding Author: Tel.: +1865 576 7196, E-mail address: beih@ornl.gov (H. Bei)

1.Introduction

Traditional alloys normally consist of one principle element as the predominant composition and small amounts of other additive alloying elements, such as aluminum alloys [1-4], magnesium alloys [5-7], titanium alloys [8, 9], Ni-super-alloys [10, 11] and steel [12-14]. Alloys utilized in traditional industrial applications are typically multi-phase-structured due to the requirement of mechanical or other performance requirements (e.g., high strength, oxidation resistance), which usually cannot be met by single-phase materials (e.g., pure Nickel). Recently, the alloying design strategies were extended to a group of alloys in which multiple (i.e., 5 or more) elements are present with equiatomic or near-equiatomic molar ratios [15-32]. From general physical metallurgy intuition, increasing the number of alloying elements with varying crystal structures will simultaneously increase the probability that additional phases will form. However, numerous experimental and theoretical investigations have shown that these *compositionally-complex* alloys containing multiple constituent elements in equiatomic or near-equiatomic concentrations tend to crystallize as *structurally-simple* solid solutions with promising properties [16-18]. One representative *compositionally-complex* but *structurally-simple* alloy is the equiatomic high entropy alloy FeNiCoCrMn, which was found to exhibit single-phase with FCC crystal structure. This alloy was first explored in 2004 by Cantor et al. [19] after which various properties of this alloy have been investigated, such as thermodynamic stability [21], malleability [22], and diffusion kinetics [24]. This alloy attracted both practical and scientific interests from a few perspectives. Its yield strength showed an intermediate temperature-dependence that is between pure FCC and BCC metals which was suggested to be determined by Peierls-

barrier-dominated lattice friction, with the height of the Peierls barrier controlled by thermal influences on the width of the dislocation [25]. Another interesting observation in this alloy is that, contrary to most traditional materials in which an inverse temperature-dependence of strength and ductility is usually seen [33], the remarkable increase in strength was accompanied by a substantial increase in ductility with decreasing deformation temperature (e.g., from 293 to 77 K). A superior fracture toughness, as high as 200 MPa.$m^{1/2}$, comparable to the very best cryogenic steels (e.g., austenitic stainless steels and high-Ni steels) at 77 K was also reported [34].

Due to their superior overall mechanical properties, these alloying systems could be important structural materials for advanced nuclear reactor and power plants in which commercial steel grades, including 304, 316, 321, and 347 were typically used due to their high malleability (e.g., rolling, bending and forging), good combinations of strength and ductility at both high and low temperatures and high corrosion resistance [35-38]. However, information regarding the structural stability and mechanical properties degradation under irradiation is limited for multi-component alloys. It is hypothesized that the high configurational entropy of these alloys might promote point defect recombination and compositional reordering following energetic displacement cascade events, but there are no experimental data available. In order to identify the potential of using these alloys in reactors, it is important to conduct a thorough investigation of the neutron irradiation effects on their structure and properties. The FeNiCrCoMn must be excluded from neutron-irradiation investigation since the presence of 25 at. % Co as one of the principle elements makes post-neutron-irradiation testing very difficult due to the production of high levels of the ^{60}Co radioisotope during neutron irradiation. Therefore,

to facilitate radiation damage testing on multi-component alloys, new alloys that do not contain high-activation elements such as Co need to be developed as low activation materials.

The purpose of this study is to develop a *compositionally-complex* but *structurally-simple* material containing no Co, but with comparable mechanical properties to the equiatomic FeNiCoMnCr alloy. The simplest way to achieve this goal is to directly remove Co from the equiatomic FeNiCoMnCr alloy. However, the resulting quaternary equiatomic FeNiMnCr alloy was shown to exhibit a multi-phase microstructure under homogenization conditions [22]. Thus in the current study, the molar concentration of the BCC-stabilizer Cr [39] will be reduced while the atomic ratio of the other three elements, Fe, Ni and Mn, will be maintained equiatomic. It has been shown that, to stabilize the FCC austenite, the amount of Cr should not exceed 18 wt.% [40] otherwise austenite will be destabilized by the presence of Mn. Since all the elements, Fe, Ni, Mn and Cr, have similar molar weight, in the current investigation, the concentration of Cr will be set as 18 at.%. The microstructures and mechanical properties of the resultant $FeNiMnCr_{18}$ alloy will be investigated and compared to the equiatomic FeNiCoMnCr high entropy alloy.

2. Experimental Methods

2.1. Alloy Preparation

The near-equiatomic $FeNiMnCr_{18}$ alloy was produced by arc melting the raw materials of Fe, Ni, Cr, and Mn (>99.9% pure) in a water-cooled copper hearth under Ar atmosphere. The arc-melted buttons were flipped and re-melted at least five times to

promote thorough mixing and then drop-cast into copper molds to produce ingots measuring 12.7 mm × 12.7 mm × 70 mm. The drop-cast ingots were homogenized for 24 hours at 1200 ^{o}C, followed by water quenching. The ingot was then cold rolled along the longitudinal ingot direction to a total thickness reduction of 86% without cross-rolling or intermediate annealing. Pieces cut from the cold-rolled ingots were annealed to investigate its recrystallization and grain growth behavior.

2.2. Tensile Tests

Flat dog-bone-type specimens with a gage length of 10 mm were cut from the cold-rolled sheets by electrical discharge machining (EDM) with their longitudinal axes perpendicular to the rolling direction. The specimens were annealed at 900 ^{o}C for 1 hour, and all faces of their gage sections ground through 600-grit SiC paper. Nine Vickers microhardness indents spaced 1 mm apart were made along the specimen gage lengths using a LECO LM 100_{AT} Vickers Hardness tester with a force of 200 g. The change in the distance between adjacent indents, excluding the two indents on either side of the fracture plane, was used to calculate the uniform elongations to fracture.

Tensile tests were performed with an Instron screw-driven tensile testing machine at an engineering strain rate of 10^{-3} s^{-1} and temperatures of 77, 293, 473, 673, and 873 K. For the tests at 77 K, the specimens and grips were first fully immersed in a bath of liquid nitrogen for about 15 minutes before starting the test. During the tests, the baths were continuously filled as needed to keep the specimen and grips fully immersed at all times. Room-temperature and above tests were performed in ordinary ambient air. Two nominally identical specimens of each alloy were tested at each temperature.

2.3. Microstructure Characterizations

Crystal structures of the as-cast, homogenized, cold-rolled and annealed, and the tensile-deformed samples were examined by x-ray diffraction with Cu-target radiation at 40 kV and 40 mA. The samples were scanned through 2θ ranging from 30 to 90 degrees with a scan rate of 1.2 degrees/minute.

6500F JEOL FEG-SEM equipped with a TSL OIM system was used to characterize the microstructures of the as-annealed and tensile-fractured materials. The elecron backscatter diffraction (EBSD) measurements were performed with an electron probe current of 3.0 nA at an acceleration voltage of 20 kV, with step size of 300 nm (low magnification) or 20 nm (high magnification). The qualification and analysis of the EBSD results were performed using TSL OIM V7^{TM} software. EBSD maps are displayed as inverse pole figure (IPF) maps in the direction of the rolling direction (for the initial microstructure) or tensile axis (for the tensile-deformed microstructure). Data "cleaning" procedures were not used [41].

3. Results

Figure 1*a* shows the x-ray diffraction pattern of the $FeNiMnCr_{18}$ material after homogenization at 1200 ^{o}C for 24 hours. Unlike the equiatomic FeNiMnCr alloy which exhibits multi-phase microstructure under homogenization [22], only FCC peaks were observed in the homogenized near-equiatomic $FeNiMnCr_{18}$ alloy, indicating the nature of being single FCC phase solid solution. To further confirm the single-phase nature, careful microstructure examination was conducted, Figure 1*b* and 1*c* shows representative microstructures of the near-equiatomic $FeNiMnCr_{18}$ alloy in the cast and homogenized states. The as-cast specimen consists of large elongated grains (Fig. 1*b*) extending from

the edges to the center of the rectangular cross-section molds, consistent with the heat flow directions during solidification. After homogenization at 1200 ^{o}C for 24 h, near the center of the casting ingot, the elongated grains are replaced by more equiaxed grains (Fig. 1*c*). After cold rolling and annealing at 900 °C for 1 hour, both the x-ray diffraction pattern (Fig. 2*a*) and the electron backscatter diffraction (EBSD) inverse pole figure (IPF) map (Fig. 2*b*) reveal the presence of only FCC solid solution phase. While maintaining the single-phase feature, the microstructures of this alloy are highly thermomechanically controllable. As can be seen, the annealed material is fully recrystallized and contains homogeneous equiaxed grain microstructure without strong texture. Annealing twins can be observed in many grains. The average grain size without twin boundaries determined by a linear intercept method was found to be 15 μm. After tensile testing at all temperatures, X-ray diffraction failed to detect any phase transformation or second-phase precipitation, indicating that the FCC single-phase structure remained stable during deformation.

Figure 3*a* shows the representative engineering stress-strain curves for the $FeNiMnCr_{18}$ alloy at the five test temperatures. Only the plastic components of the tensile load-displacement data, which were calibrated using the measured uniform elongation of the gage length determined from the microhardness indents, were presented. The plastic strain was obtained by fitting a straight line the linear elastic portion of the curves and subtracting the elastic strain at a given point on the curve from the total strain. Figure 3*b-d* summarize the 0.2% offset yield strengths (σ_y), ultimate tensile strengths (*UTS*), and uniform elongations to fracture (e_f). Values obtained from two different samples were presented to confirm the date reproducible. For the purpose of comparison, data for the

equiatomic FeNiCoCrMn alloy with similar grain size (~ 35 μm) are also presented (Fig. 3*b-d*). The values for both alloys are generally comparable and similar temperature-dependence trend is observed. For both alloys, the highest values of yield strength; ultimate tensile strength and elongation to fracture are all obtained at liquid nitrogen temperature (77 K). An increase in temperature results in a monotonic decrease in both the yield and ultimate tensile strengths. Similar case was also observed for the uniform elongation, however, a minimum in ductility occurs in the intermediate temperature range (around 473 K) for the $FeNiMnCr_{18}$ alloy.

4. Discussion

The strong temperature dependencies of yield strength, which is not typical for pure FCC metals, such as Ni and Cu, in the equiatomic FeNiCoCrMn alloy and its various equiatomic was expected to be caused by the variation of Peierls-barrier-dominated lattice friction with temperature due to the control of the height of the Peierls barrier (which was shown to be stronger than those in pure FCC metals but weaker than those in pure BCC metals) by thermal influences on the width of the dislocation. Our near-equiatomic $FeNiMnCr_{18}$ alloy has similar temperature dependencies of yield strength; however, whether or not the same mechanism is applicable to this alloy is beyond the scope of current study. Further microstructural and mechanistic investigations will be needed in order to have a thorough appreciation of this. Detailed microstructural characterization has been performed to have a deeper understanding of the effects of temperature on UTS in the equiatomic FeNiCoMnCr alloy [26]. The formation of nano-twinning during deformation (after ~ 20% strain) and the activation of additional

twinning systems at higher strain (e.g., beyond ~ 38% engineering strain) in the {1 1 1} twinning planes were believed to be important contributors to the large strain hardening capabilities and hence UTS at lower temperatures (e.g., 77 K) due to their capabilities of acting as additional deformation mode [26]. In order to have a better understanding of the observed temperature dependence of UTS in the current $FeNiMnCr_{18}$ alloy, the extent of work hardening, defined here as the differences between UTS and yield strength, was also plotted as a function of temperature (Fig. 4). Generally, the work hardening capability of the $FeNiMnCr_{18}$ alloy also decreases with increasing temperature with the largest differences happen between 293 and 77 K. The work hardening capability of the $FeNiMnCr_{18}$ alloy (~ 490 MPa) is slightly lower than that of the equiatomic FeNiCoCrMn alloy (~ 580 MPa).

To provide a microstructure-based understanding of the observed mechanical behavior, the microstructures of the investigated near-equiatomic $FeNiMnCr_{18}$ alloy were characterized as a function of temperature. The EBSD maps showing the microstructures of the $FeNiMnCr_{18}$ alloys tensile-deformed to fracture under different temperatures were shown in Figure 5*a*-*e*. Compared to the initial as-annealed material (Fig. 2*b*), which shows nearly equiaxed grain structures and constant in-grain orientation, under fracture, the grains become elongated along the tensile direction and significant orientation fluctuations appear. These in-grain orientation variations could be caused by the accumulation and increased density of the stored dislocations with the level of the plastic deformation [42].

The microstructure of the material tensile-fractured at 77 K has a zig-zag-shaped and colony-like morphology which is full of parallel bands with various thickness and

spacings (Fig. 5*a*). To have a better visualization and understanding of these bands, slow scan with a step size of 20 nm was conducted under high magnification. Figure 6*a* shows the corresponding high-magnification Kikuchi pattern quality (KPQ) map composed of a few visible straight dark lines in a semi-micron-scale band. To identify details of these bands, a red line crossing the band was drawn and misorientations along the red line were measured and plotted (Fig. 6*b*). It shows that whenever the line passes the individual band there will be a 60^{o} misorientation, indicating that these bands are composed of Σ3 twins. Worth to note that some smaller bands may be missed due to the limited spatial resolution of EBSD. The formation of these nano-sized twins may occur at the early stage of deformation and they starts to bundle and form twin bands with the level of plastic deformation increased. The twins generated from different systems will interact with each other and make a zig-zag-like microstructure (Fig. 5*a*). The densities of the twin bands are largely reduced when the test temperature is increased: no twin bands are observed when the temperature is further increased to 293 K and higher (Fig. 5*b*-*e*). The twinning activities may be influenced by the deformation temperature through several different ways. First, the reduced dynamic recovery and enhanced yield strength (Fig. 3*a*) under lowered temperatures (e.g., 77 K) will make the critical stress that needs to be reached in order to activate deformation twinning easier to be achieved. Deformation temperature will also change the stacking fault energy of materials which will resultantly affect the twinning activities: decrease of stacking fault energy at lower temperature will cause more pronounced twinning.

Another striking feature is that, for tests under all five temperatures, under failure, the highly-distorted grains tend to exhibit orientations mainly with the <1 1 1>- or <1 0 0>-

crystallographic direction parallel to the tensile axis. Twinning is also found to strongly dependent on the orientation. For tensile deformation under 77 K in which twinning is visible, it is clear that twinning mostly occurs on the <1 1 1>//TA oriented grains and those with certain deviations. Similar orientation-dependence of twinning have also been reported by previous studies on face-centered cubic metal and alloys, including Ag–Au alloys [43], Cu [44], and polycrystalline Fe-33Mn-3Al-3Si [45], Fe-31Mn-3Al-3Si [46], and Fe-22Mn-0.6C [47] twin-induced-plasticity (TWIP) steels. In all of these investigated materials, mechanical twinning readily occurred when the tensile axis lay near [1 1 1] direction, whereas no deformation twinning was observed for the orientation lying near the [0 0 1]. These dependencies of the twinning activation on the grain orientation have been explained by assuming that there is an identical critical resolved shear stress for slip and mechanical twinning. In this case, preferred and dominant deformation mechanism will be different for grains with different orientations and the comparison of the Schmid factors for dislocation slip and mechanical twinning could be helpful for evaluating this [45, 47, 48]. Under tension, grains with their <1 1 1> directions aligned to the tensile axil (TA) (<1 1 1>//TA) have larger Schmid factor for the mechanical twinning (0.31) than that for dislocation slip (0.27); while <0 0 1>//TA oriented grains have a larger Schmid factor for dislocation slip (0.41) than that for deformation twinning (0.24) [48]. Additional explanation is based on the assumption that the activation and formation of deformation twinning is governed by the dissociation of glide dislocations into Shockley partials only [49]. In this case, the degree of separation of two moving Shockley (leading and trailing) partials will be one of the most important factors which determine the tendency of twinning. It was suggested that the steady-state separation (width of partial

separation) of a glide dislocation could show strong orientation dependence. In <1 1 1> oriented grains, the occurrence of complete dissociation of the Shockley pair will accompany with the production of stacking faults, but in <0 0 1> oriented grains, the dislocation pair will experience a constriction [50, 51]. Convincing microstructural evidences showed that these generated stacking faults could serve as precursors for nano-scaled deformation twins [52]. Further study is needed to clarify these.

Based on the above-mentioned observations, the strong dependencies of strain hardening on temperature could, similar to the equiatomic FeNiCoCrMn alloy, also be attributed to the enhanced twinning activities at lower temperatures. Thin nano-twins formed during deformation will be able to serve as obstacles to dislocation motion even when they are separated distributed without being bundled. They can act as even stronger obstacles than single twins once they are arranged in bundle (as observed in Fig. 5*a* and 6*a*) due to the higher critical stress required to carry plastic deformation across the twin bundle than that required to penetrate an individual twin [53, 54]. Furthermore, interactions between dislocations and twins will cause the accumulation of a high density of sessile dislocations within the twin lamellae, leading to increased twin strength with deformation. These accumulated dislocations are potentially effective barriers to dislocation motion and can provide additional strengthening within the induced mechanical twins and increase the critical stress required to induce plastic deformation across the twins. A map revealing short-range orientation gradients were shown in Figure 7*a* to support the hypothesis of dislocation accumulation around the twin boundaries. The orientation gradients were highlighted using the Kernel parameter for the first neighbors which is the average misorientation angle between the current pixel orientation and its six

first neighbors. Higher values of orientation variations were observed near twin boundaries. Possible cause of this observation is the twin-slip interactions and this may indicate the dislocation pile-up at the twin boundaries. Figure 7 also shows that, upon failure at 77 K, their microstructures are separated by twin (lamellae) boundaries into tiny twin-free areas. This should be caused by the development of dense twin substructure, the cutting of twin boundaries through dislocation substructure and the interactions between primary and secondary twinning systems. Due to the capability of the deformation-twin boundaries to serve as dislocation-motion obstacles, the "effective grain size" will be much smaller than the real measured grain size since each twin-surrounded area will act as a "grain". The effect is often referred to as a "dynamic Hall-Petch effect" [55-60] which can significantly contribute to the enhanced strain hardening. Besides the above-mentioned strain-hardening, the formation of deformation twinning will also postpone the necking stability and hence increase the ductility, causing the uniform elongation to increase with the decrease of temperature instead of being inversely dependent on the strength, which disobey the generally accepted rule that the increase of strength should be at the expense of ductility. This can be supported by the representative fracture surfaces of $FeNiCMnCr_{18}$ alloy shown in Figure 8 which shown much less necking under 77 K (Fig. 8*a*) than that under 293 K (Fig. 8*c*), even both show typical ductile dimple fractograph (Fig. 8*b* and *d*).

The mechanical twinning as additional deformation mode can also explain the observed difference in the mechanical properties of the equiatomic FeNiCoCrMn and near-equiatomic $FeNiCMnCr_{18}$ alloys (e.g., strain hardening and elongation). The equiatomic FeNiCoCrMN alloy hold slightly larger values of strain hardening capability

and uniform elongation under 77 K than those of near-equiatomic $FeNiCMnCr_{18}$ alloys. Deformation twinning ability and activities has been shown to be strongly dependent on the stacking fault energy of materials. Twinning tend to occur and to be a major deformation mode for FCC meals and alloys with low stacking fault energy (γ_{SFE}), such as 70:30 brass [61], but not typical for face-centered cubic (FCC) metals with medium or high stacking fault energy, such as Al [62]. Previous studies have even reported a critical value of ~ 45 mJ/m^2 of stacking fault energy value determining whether or not twinning will occur in FCC materials. With higher stacking fault energy (> 45 mJ/m^2), the twining will not occur and deformation will be solely controlled by dislocation glide; while with a reduced stacking fault energy (< 45 mJ/m^2), the deformation mode will transit from dislocation glide to deformation twinning; while the stacking fault energy was further reduced (< 18 mJ/m^2), martensitic transformation will become the favorable mechanism controlling the deformation [63, 64]. Previous studies have also shown that the addition of Fe, Co, Cr and Mn to pure Ni will all reduce its stacking fault energy with Cr has the largest effect and Fe the smallest [65, 66]. So it is reasonable to expect a relatively higher stacking fault energy of $FeNiMnCr_{18}$ alloy compared to that of the equiatomic FeNiCoCrMn alloy due to the more concentration of Cr and Co.

4. Summary and Conclusions

We have developed a multi-component near equi-atomic compositionally complex $FeNiMnCr_{18}$ solid solution alloy (without element Co) with simple FCC crystal structure, which allows post-neutron-irradiation testing. The $FeNiMnCr_{18}$ alloy was cast, homogenized, cold-rolled and annealed. Its microstructures and mechanical properties

were investigated as a function of temperature. Based on this study, the following conclusions can be drawn:

(1) A FCC-structured single-phase alloy with a composition of $FeNiMnCr_{18}$ was developed. FCC single-phase structure remained stable during deformation.

(2) The near-equiatomic $FeNiMnCr_{18}$ alloy has good malleability and its microstructure can be thermomechanically controlled. By rolling and annealing, the as-cast elongated-grained-microstructure is replaced by homogeneous equiaxed grains.

(3) The mechanical properties (e.g., strength and ductility) of the $FeNiMnCr_{18}$ alloy are comparable to those of the quinary equiatomic FeNiCoMnCr alloy. Both strength and ductility have strong temperature dependencies.

(4) In the near-equiatomic $FeNiMnCr_{18}$ alloy, extensive twin-bands which are bundles of numerous individual twins are observed when it is tensile-fractured at 77 K. No twin bands are detected by EBSD for materials deformed at 293 K and higher.

(5) When the material is deformed at 77 K, the development of a dense twin substructure, twin-dislocation interactions and the interactions between primary and secondary twinning systems result in microstructure refinement, and hence cause enhanced strain hardening and postponed necking, resulting in negative temperature-dependencies of UTS and uniform elongation.

Acknowledgments

This work was supported by the Department of Energy, Office of Sciences, Basic Energy Science, Materials Science and Engineering Division.

References

[1] Hahn GT, Rosenfield AR. Metall Trans A 1975; 6(4): 653.

[2] Wu ZG, Song M, He YH. Mater Sci En A 2009; 504: 183.

[3] Song M, Wu Z, He Y. Mater Sci En A 2008; 497: 519.

[4] Christman T, Suresh S. Acta Metall 1988; 36(7): 1691.

[5] Gong X, Kang SB, Li S, et al. Mater Design 2009; 30 (9): 3345.

[6] Gong X, Li H, Kang SB, Cho JH, et al. Mater Design 2010; 31 (3): 1581.

[7] Hu HJ, Fan JZ, Zhai ZY, et al. Russ J Non-ferr Met 2014; 55 (3): 254.

[8] Sun P, Fang ZZ, Koopman M, et al. Acta Mater 2015; 84: 29.

[9] Sun P, Fang ZZ, Koopman M. Adv Eng Mater 2013; 15: 1007.

[10] Chen X, Sokolov MA, Sham S, et al. J Nucl Mater 2013; 432 (1): 94.

[11] Chen X, Yang Z, Sokolov MA, et al. Mater Sci Eng A 2013; 563: 152.

[12] Hall EO. Proceedings of the Physical Society of London Section B 1951; 64(381): 747.

[13] Bhadeshia H, Edmonds DV. Metall Trans A 1979; 10:895.

[14] Chen X, Stubbins JF, Hosemann P, et al. J Nucl Mater 2010; 398(1): 172.

[15] Yeh JW, Chen SK, Lin SJ, et al. Adv Eng Mater 2004; 6: 299.

[16] Senkov ON, Scott JM, Senkova SV, et al. J Alloys Compd 2011; 509: 6043.

[17] Guo S, Liu CT. Prog Nat Ssi 2011; 21(6): 433.

[18] Yang X, Zhang Y. Mater Chem Phys 2012, 132(2–3): 233.

[19] Cantor B, Chang ITH, Knight P, et al. Mater Sci Eng A 2004; 375-377: 213.

[20] Guo W, Dmowski W, Noh JY, et al. Metall Mater TransA 2013; 44(5): 1994.

[21] Otto F, Yang Y, Bei H, et al. Acta Mater 2013; 61(7): 2628.

[22] Wu Z, Bei H, Otto F, et al. Intermetallics 2014; 46: 131.

[23] Liu WH, Wu Y, He JY, et al. Scripta Mater 2013; 68:526.

[24] Tsai KY, Tsai MH, Yeh JW. Acta Mater 2013; 61: 4887.

[25] Wu Z, Bei H, Pharr GM, et al. Acta Mater 2014; 81:428.

[26] Otto F, Dlouhy A, Somsen Ch, et al. Acta Mater 2013; 61: 5743.

[27] Xu XD, Liu P, Guo S, et al. Acta Mater 2015; 84: 145.

[28] Ma SG, Liaw PK, Gao MC, et al. J Alloys Compd 2014; 604: 331-339.

[29] Ma SG, Zhang Y. Mater Sci Eng A 2012; 532: 480.

[30] Bei H. US Patent 2013/0108502 A1.

[31] Zhu C, Lu ZP, Nieh TG. Acta Mater 2014; 68:214.

[32] Antonaglia J, Xie X, Tang Z, et al. JOM 2014; 66(10):2002.

[33] Dieter GE. Mechanical metallurgy. McGraw-Hill Higher Education; 1986.

[34] Gludovatz B, Hohenwarter A, Catoor D, et al. Science 2014; 345: 1153.

[35]Maziasz PJ, Busby JT. Properties of Austenitic Steels for Nuclear Reactor Applications. Elsevier Ltd

[36] Piatti G, Schiller P. J Nucl Mater 1986; 141-143: 417.

[37] Washko SD, Aggen G. In Metals Handbook: Properties and Selection: Irons, Steels, and High-Performance Alloys, 10th ed.; ASM International: Materials Park, OH, 1990; Vol. 1.

[38] Lula RA. Ed. Stainless Steel; ASM International: Materials Park, OH, 1986.

[39] Hosford WF. Physical Metallurgy. CRS Press 2005.

[40] Raghavan V. Metallurgical and Materials Transactions A 1995; 26: 237.

[41] Brewer LN. Michael JR. Microscopy Today 2010; 18: 10-15.

[42] Kamaya M. Wilkinson AJ, Titchmarsh JM. Nucl Eng Design 2005; 235: 713.

[43] Suzuki H, Barrett CS. Acta Metall 1958;6:156.

[44] Blewitt TH, Coltman RR, Redman JK. J Appl Phys 1957; 28: 651.

[45] Yang P, Xie Q, Meng L, et al. Scripta Mater 2006; 55: 629.

[56] Ueji R, Tsuchida N, Terada D, et al. Scripta Mater 2008; 59: 963.

[47] Gutierrez-Urrutia I, Zaefferer S, Raabe D, Mater Sci Eng A 2010; 527: 3552.

[48] Lee YK. Scripta Mater 2012; 66: 1002.

[49] Copley SM, Kear BH. Acta Metall 1968; 16: 227.

[50] Goodchild D, Roberts WT, Wilson DV. Acta Metall 1970; 18: 1137.

[51] Kestenbach HJ. Phil Mag 1977; 36: 1509.

[52] Idrissi H, Ryelandt L, Veron M, et al. Scripta Mater 2009; 60: 941.

[53] Christian JW, Mahajan S. Prog Mater Sci 1995; 39: 1.

[54] Reed-Hill RE, Hirth JP, Rogers HC. Deformation Twinning. Gordon and Breach Science

[55] Rémy L. Acta Metall 1978; 26: 443.

[56] Asgari S, El-Danaf E, Kalidindi R, Doherty R. Metall Mater Trans A 1997; 28: 1781.

[57] Rohatgi A, Vecchio KS, Gray GT. Metall Mater Trans A 2001; 32: 135.

[58] Beladi H, Timokhina IB, Estrin Y, et al. Acta Mater 2011; 59: 7787.

[59] Rémy L, Pineau A. Mater Sci Eng 1976; 26: 123.

[60] Gutierrez-Urrutia I, Raabe D. Acta Mater 2011; 59: 6449.

[61] Hatherly M. in: Gifkins RC. Strength of Metals and Alloys (ICSMA 6), Vol. 3, Pergamon Press, Oxford, 1982, 1181.

[62] Huang CX, Wang K, Wu SD, et.al. Acta Mater 2006; 54: 655.

[63] Curtze S, Kuokkala VT. Acta Mater 2010; 58: 5129.

[64] Frommeyer G, Brüx U, Neumann P. ISIJ International 2003; 43: 438.

[65] Kotval PS, Nostor OH. TMS-AIME 1969; 245: 1275.

[66] Gallagher PCJ. Metall Trans 1970; 1: 2429.

Figure Captions:

Fig. 1. (a) X-ray diffraction pattern of the of $FeNiMnCr_{18}$ alloy homogenized at 1200 ^{o}C for 24 hours after casting; the back-scattered electron images of the $FeNiMnCr_{18}$ alloy under (b) as-cast and (c) homogenization condition.

Fig. 2. (a)X-ray diffraction pattern and (b) microstructure of $FeNiMnCr_{18}$ alloy annealed at 900 ^{o}C for 1 hour after cold-rolling; coloring is the inverse pole figure map projected on rolling direction (horizontal)

Fig. 3. (a) Representative engineering stress *vs.* plastic strain, (b) 0.2% offset yield strengths (σ_y), (c) ultimate tensile strengths (UTS), and (d) uniform elongations to fracture (e_f) as a function of temperature for $FeNiMnCr_{18}$ alloy; data for the equiatomic FeNiCoMnCr alloy [26] were also presented for comparison.

Fig. 4. Strain hardening capability as a function of temperature for $FeNiMnCr_{18}$ alloy; data for the equiatomic FeNiCoMnCr alloy [26] were also presented for comparison.

Fig. 5. EBSD images of $FeNiMnCr_{18}$ alloy shows the microstructures of the tensile-fractured samples deformed at (a) 77K, (b) 293 K, (c) 473 K, (d) 673 K, and (e) 873 K. Coloring is the inverse pole figure map projected on tensile direction.

Fig. 6. (a) High-magnification Kikuchi pattern quality (KPQ) map of $FeNiMnCr_{18}$ alloy tensile-deformed to fracture at 77 K; (b) corresponding misorientation as a function of distance for the red line.

Fig. 7. (a) The kernel average misorientation map showing the degree of orientation gradients between the current pixel orientation and its six first-nearest neighbors, and (b) the combined index of image quality and inverse pole figure (projected onto tensile axil) map of the selected area.

Fig. 8. Fracture surfaces of the $FeNiMnCr_{18}$ alloy tensile-deformed at 77 K (a, b) and 293 K (c, d).

Figure-1

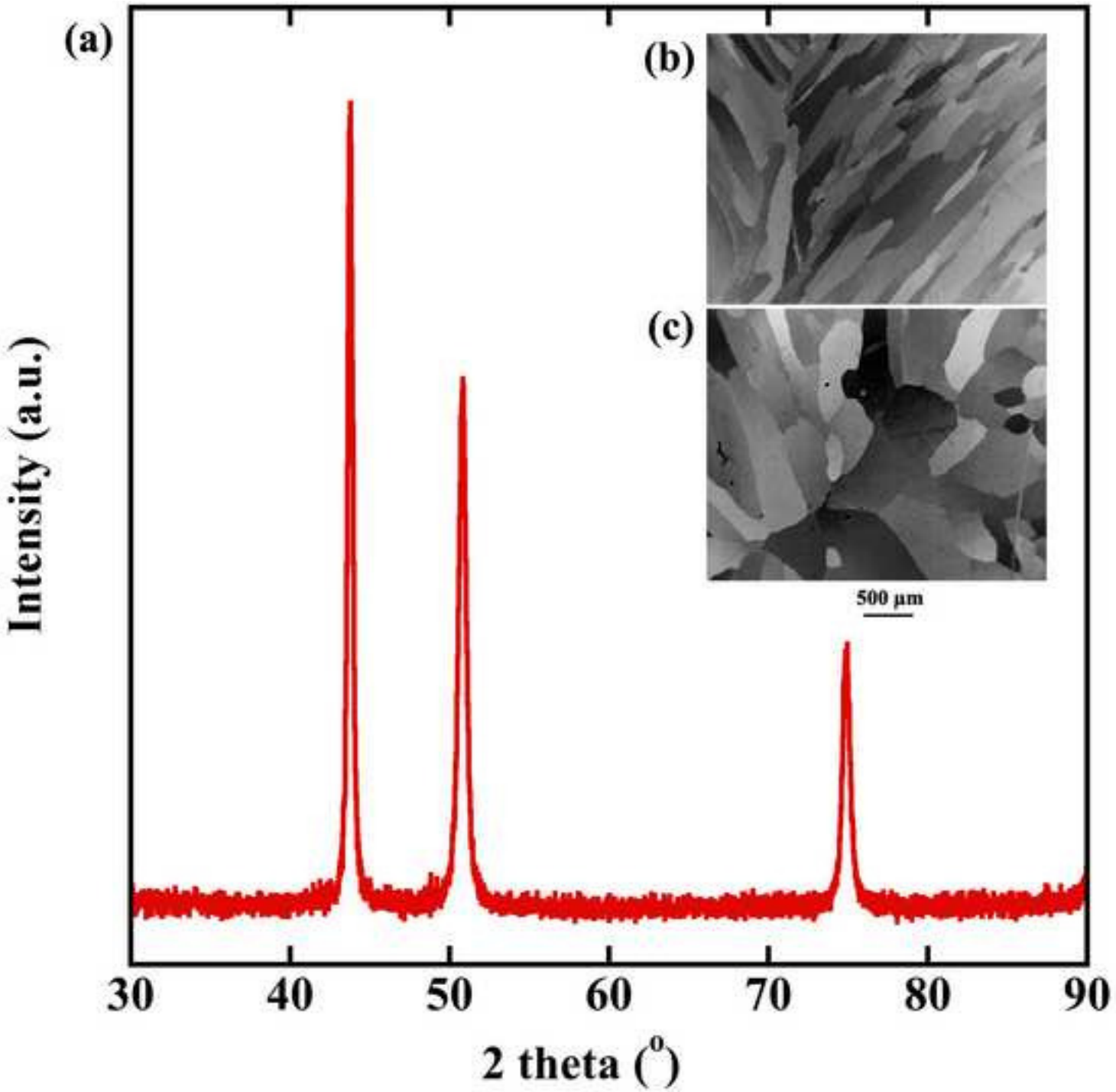

Figure-2

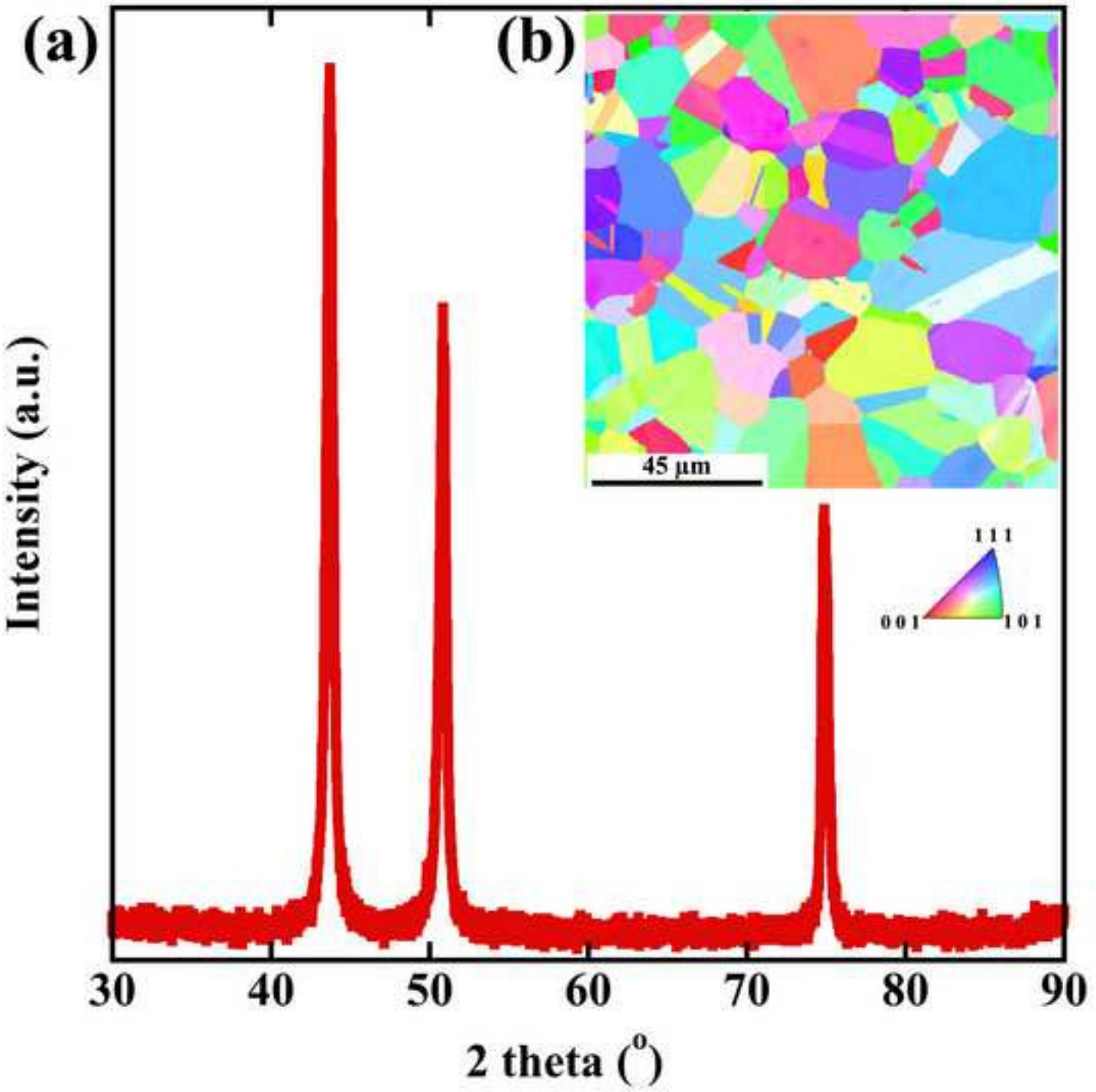

Figure-3

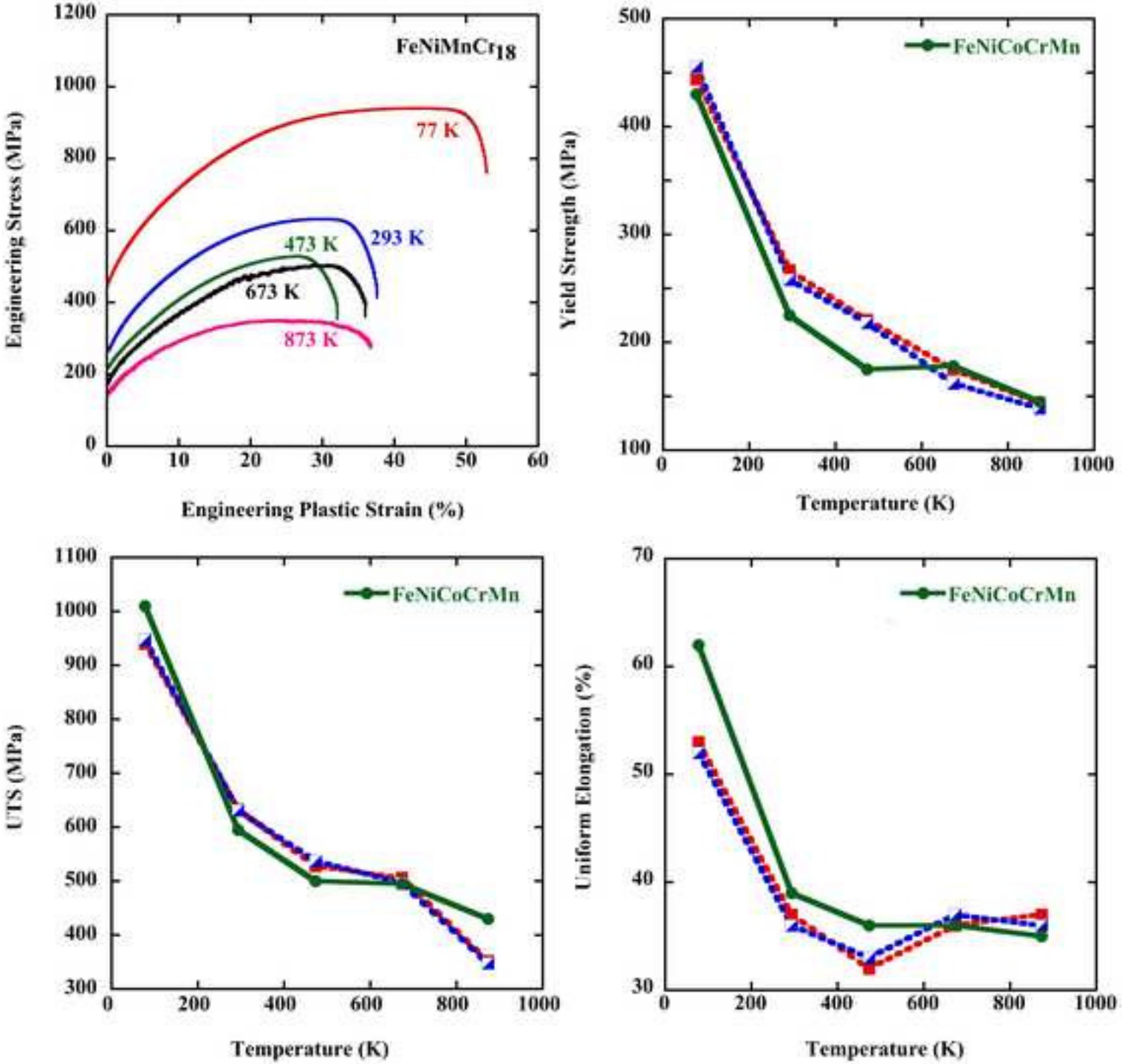

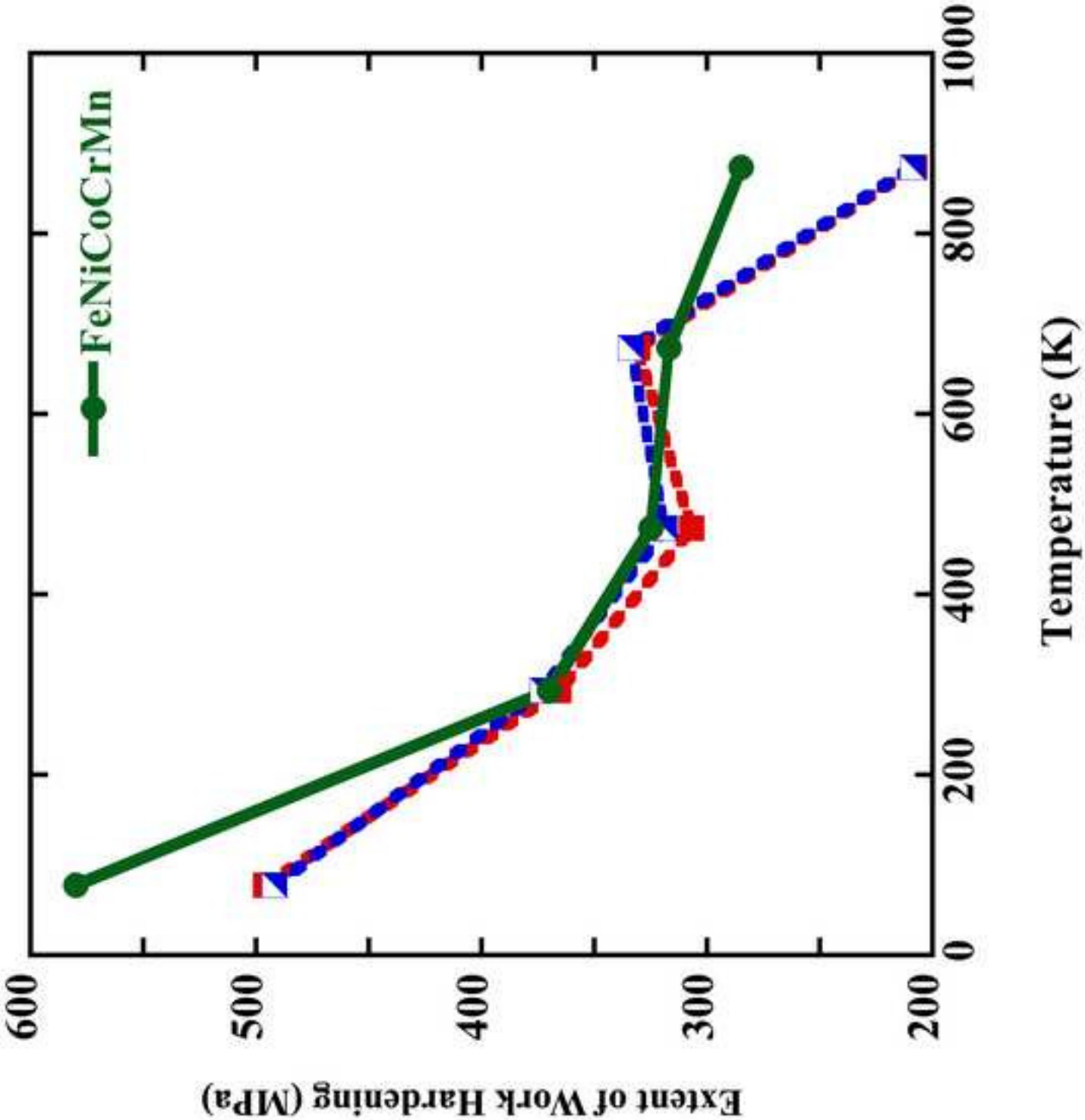

Figure-4

Figure-5

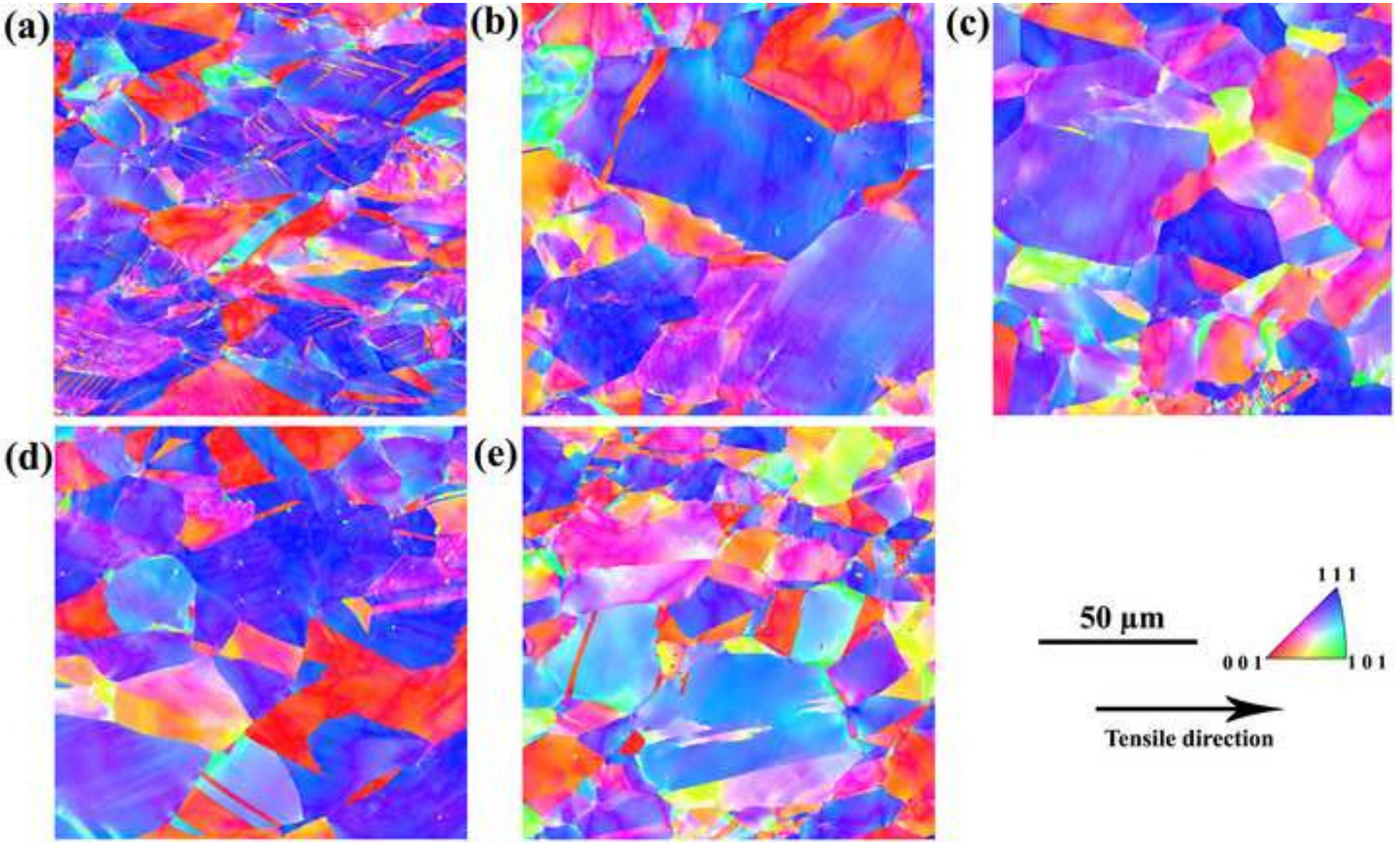

Figure-6

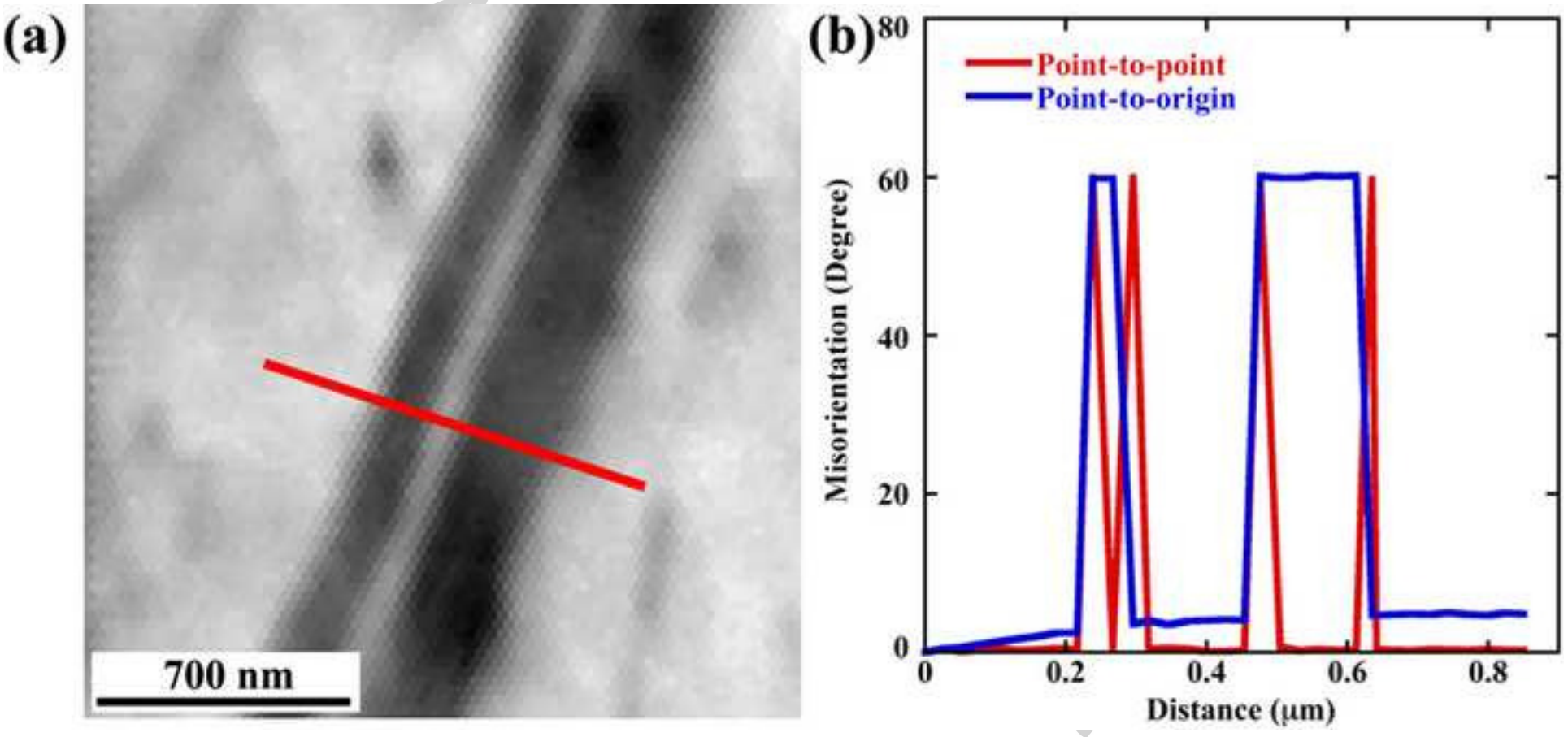

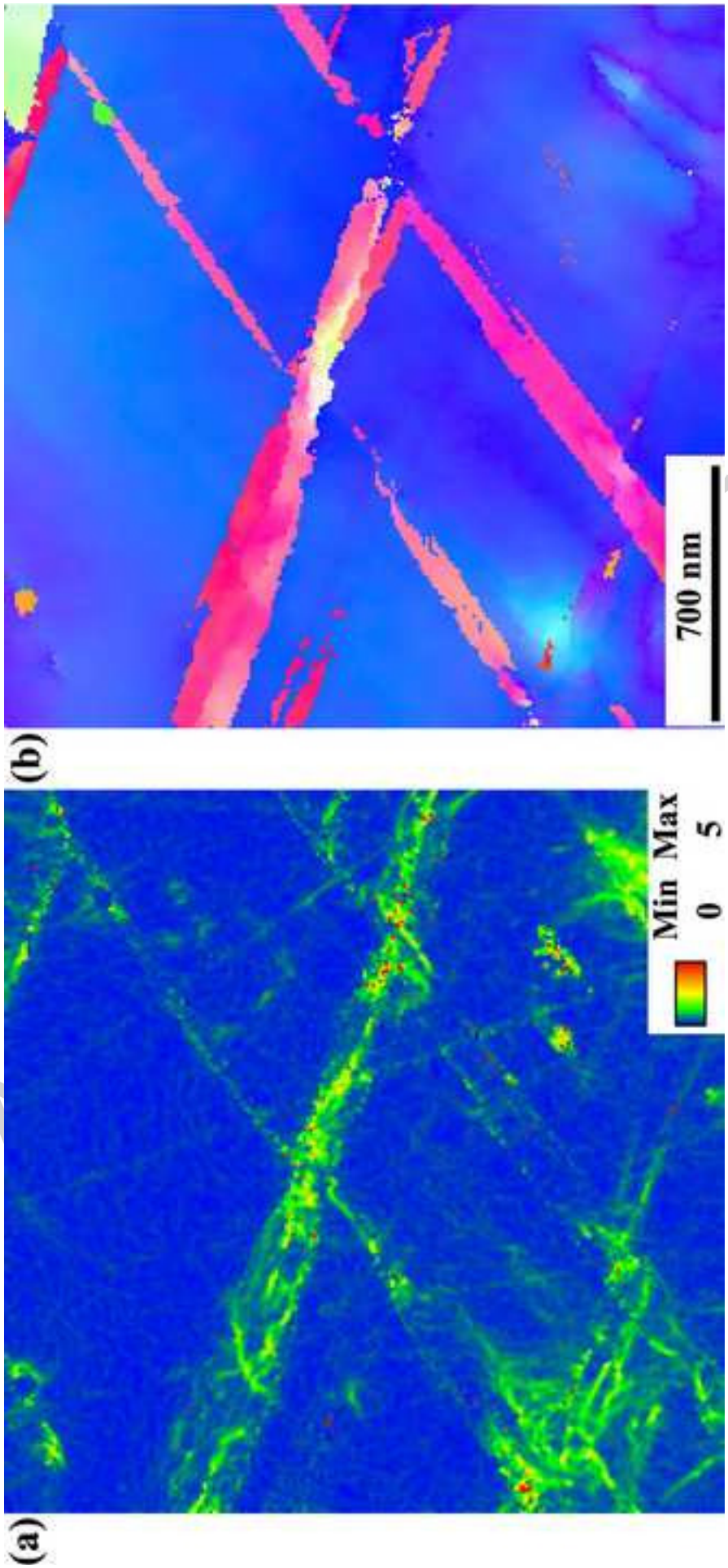

Figure-7

Figure-8